Radial density distribution of a warm dense plasma formed by underwater electrical explosion of a copper wire

M. Nitishinskiy, D. Yanuka, A. Virozub, and Ya. E. Krasik
Physics Department, Technion, Haifa 32000, Israel

(Received 27 July 2017; accepted 3 November 2017; published online 8 December 2017)

Time- and space-resolved evolution of the density (down to 0.07 of solid state density) of a copper wire during its microsecond timescale electrical explosion in water was obtained by X-ray back-lighting. In the present research, a flash X-ray source of 20 ns pulse-width and >60 keV photon energy was used. The conductivity of copper was evaluated for a temperature of 10 kK and found to be in good agreement with the data obtained in earlier experiments [DeSilva and Katsouros, Phys. Rev. E **57**, 5945 (1998) and Sheftman and Krasik, Phys. Plasmas **18**, 092704 (2011)] where only electrical and optical diagnostics were applied. Magneto-hydrodynamic simulation shows a good agreement between the simulated and experimental waveforms of the current and voltage and measured the radial expansion of the exploding wire. Also, the radial density distribution obtained by an inverse Abel transform analysis agrees with the results of these simulations. Thus, the validity of the equations of state for copper and the conductivity model used in the simulations was confirmed for the parameters of the exploding wire realized in the present research. *Published by AIP Publishing*. https://doi.org/10.1063/1.4997893

I. INTRODUCTION

Experiments with underwater electrical wire explosions (UEWE), accompanied by phase transitions from solid state to low-ionized plasma, showed that this approach can be successfully applied for the verification of different conductivity models and equations of state (EOS) for extreme states of matter at pressures $\leq 10^{11}$ Pa, temperatures up to several eV, and a broad range of densities.[1–5]

By using magneto-hydrodynamic (MHD) simulations[6] coupled with Ohm's law, electrical circuit equations, EOS databases,[7,8] and conductivity models,[9–14] one can calculate the waveforms of the discharge current, the resistive voltage, and the radial expansion of the wire and compare these results with the experimentally obtained data. Our recent experimental research of copper and aluminum UEWE on different timescales[5,15–17] show that one obtains a good agreement between the measured wire expansion and averaged electrical conductivity and the results predicted by EOS and conductivity models only on the μs-time scale. For sub-μs timescale wire explosions, the electrical conductivity deviates from the conductivity models, resulting in values lower than those given by these models. Moreover, for ns-timescale explosion of wires, the EOS values necessary to reconstruct the experimental wire expansion were significantly different from the SESAME EOS tables and the conductivity values were significantly lower than those obtained using the conductivity models. Thus, the results of these experiments showed that the EOS and electrical conductivity models, applicable for an equilibrium state of matter, cannot be used for the correct description of the material's properties on the ns-timescale of the energy deposition. At present, there is no perfect explanation of the processes accompanying wire explosions, especially on the ns-timescale. One can only speculate that the differences between the experimental results and results of MHD simulations coupled with EOS and electrical conductivity models which are applicable for an equilibrium state of matter are the result of a transient two-phase state and/or non-uniformity of the material.

In order to confirm the validity of the conductivity models and EOS in experiments, one has to determine the time and space dependent resistance and density of the exploding wire and the deposited energy density. These time dependent parameters determine the waveforms of the discharge current $I(t)$ and the resistive voltage $\varphi(t)$, and the wire radial expansion velocity. In most experiments, the measured discharge current and voltage waveforms were used to calculate the time-dependent evolution of the average value of the wire's resistance, $R(t)$. In addition, either self-emission of the exploding wire or its shadow images were used to estimate the wire's time dependent inductance which was used to calculate the induction voltage $\varphi_{in} = -(LdI/dt + IdL/dt)$. The latter was applied to obtain the resistive voltage $\varphi_R = \varphi - \varphi_{in}$ and, consequently, the resistance, $R(t) = \varphi_R(t)/I(t)$, and the rate of the energy deposition, $\omega = I(t) \cdot \varphi_R(t)$. Here let us note that in contrast to wire explosions in gas or vacuum, in the case of UEWE, the discharge current flows through the wire because flashover discharge developing along the wire's surface is prevented by the high electric field breakdown threshold in water.[18] The resulting experimental data can be used to calculate the wire's specific resistance only if the uniform current density distribution and the absence of thermal and magneto-hydrodynamic instabilities are assumed.[19] Using these measured parameters of the exploding wire, i.e., the optically obtained wire radius and the average resistance, and the results of MHD simulations, the conductivity of copper was studied over a rather broad density (0.007–2.2 g/cm^3) and temperature (5–30 kK) range.[3,4,15–17,20–23]

To measure the time- and space-resolved radial density distribution during the wire's explosion, one can apply X-ray

backlighting to identify the density by a grayscale contrast method or the inverse Abel transform. This approach was applied for measuring the density distribution during exploding tungsten wires in vacuum using an x-pinch or a hybrid x-pinch as bright soft X-ray sources of μm scale X-ray spots and sub-nanosecond duration.[24–26] However, application of these x-pinches is challenging in experiments with UEWE because reproducible generation of hard (>50 keV) X-ray fluxes necessary to penetrate several cm of water and input windows requires additional research. Also, these sources of X-rays necessitate rather powerful high-current generators. Recently, a source of X-rays based on a vacuum diode supplied by a nanosecond high-voltage (HV) pulse generated by a compact spiral generator was used to determine the density distribution during UEWE.[27] However, because the energy of the photons was not high enough (maximum energy of X-rays was in the 50 keV range), the obtained data images allowed only to determine the radius of the exploding wire. Another approach considered radiography based on high-energy monoenergetic beams of protons with GeV-scale energy.[28] With a good quality proton beam, one can obtain, on a μm-scale, space and nanosecond timescale resolution density evolution of the exploding wire. It is understood that this approach requires very expensive equipment, a high energy charged particles accelerator, and special safety measures.

The main purpose of the present research is the investigation of time- and space-resolved density evolution during microsecond timescale UEWE. Namely, in this paper, we describe the radial density distribution of copper during UEWE obtained using back-light imaging by X-rays generated by a vacuum diode immersed in an axial magnetic field and supplied by a ~160 kV, 20 ns pulse at its Full Width Half Maximum (FWHM). The results of these experiments are compared with one-dimensional MHD simulations coupled with EOS for copper, Ohm's law, electrical conductivity models, and thermal diffusion.

II. EXPERIMENTAL SETUP AND DIAGNOSTICS

The experimental setup is shown in Fig. 1. The X-ray source is based on a vacuum diode supplied by a negative polarity high-voltage (HV) pulse (~160 kV, ~1.2 kA, and ~20 ns) produced by a solid-state semiconductor opening switch[29] based generator. The diode consists of a tungsten conical cathode (1.5 mm diameter tip) and an anode (2 mm diameter). The anode surface was oriented at ~27.5° with respect to a 5 mm thick output Perspex window. A specially made design allows the adjustment of the anode position in the x-y-z directions to an accuracy of 0.1 mm. The anode-cathode (AC) gap was ~3.0 mm in most experiments. The vacuum, 5×10^{-3} Pa, in the stainless steel chamber was kept by a turbo-molecular pump. The diode current and voltage were monitored using a B-dot loop coil and a capacitive voltage divider, respectively. An external axial magnetic field ($B = 1$ T, half period of 4 ms) was generated by two coils (see Fig. 1) installed outside the vacuum chamber. The coils were supplied by the discharge of a 4 mF capacitor charged up to 0.8 kV.

The application of the HV pulse to the cathode leads to the formation of an explosive emission plasma[30] serving as a source of electrons accelerated towards the anode. During 20 ns of the HV pulse duration, the expansion of the plasma towards the anode along the magnetic field can be estimated to be ≤2 mm,[31] and indeed the AC 3 mm gap did not short. Typical waveforms of the diode current and voltage are shown in Fig. 1(b). One can see that the amplitude of the electron current reaches 1.2 kA and the maximal voltage in the diode is ~160 kV.

A part of the flux of X-rays generated by electrons interacting with the anode and penetrating through the window was used for backlighting the exploding wire. In addition, through another output window located at the same axial distance but at 90° with respect to the Perspex window (not shown in Fig. 1), X-ray flux was monitored by a Hamamatsu R 7400U photo-multiplier tube (PMT) with a 2-mm EJ-200 scintillator covered by a 0.1-mm Al foil and placed in front of the PMT input window. The PMT was placed at a distance of 35 cm from the anode. Photon energy was estimated using X-ray flux attenuation in copper foils with different thicknesses placed in front of the PMT scintillator. The attenuation of X-ray with different energies in copper[32] together

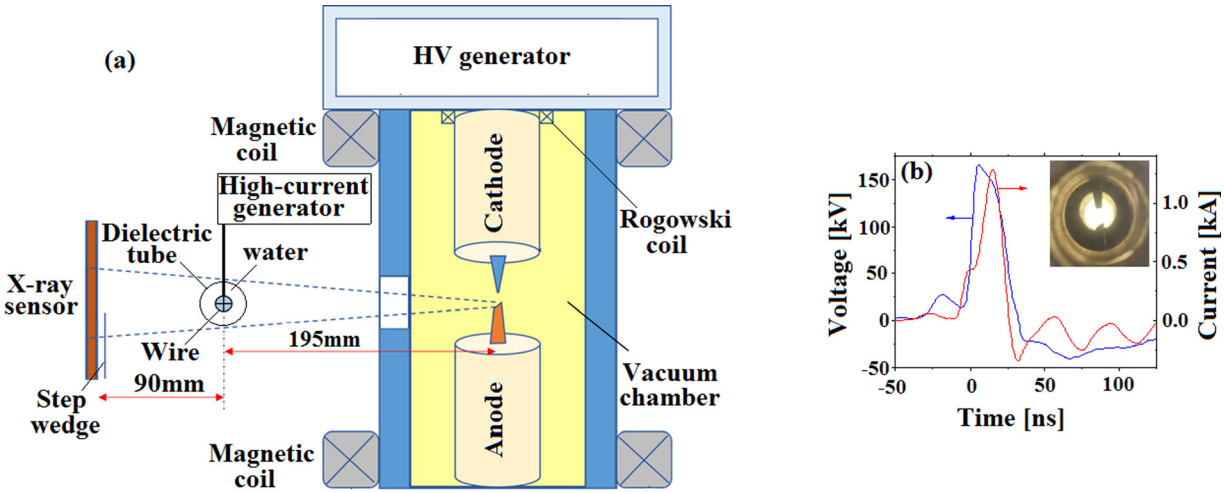

FIG. 1. (a) Experimental setup. (b) Waveforms of the current and voltage; inset: external view of the electrodes inside the vacuum chamber.

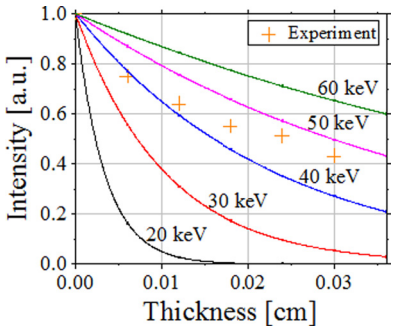

FIG. 2. Attenuation of x-rays in copper foils of different thicknesses: NIST and experimental data.

with experimental data is shown in Fig. 2. One can see (according to the slope of the curves) that a significant part of the X-rays has energy $\geq$60 keV, which matches the requirements for the X-ray source.

For static (prior to the generator short) and dynamic (during the wire explosion) x-ray images, either an X-ray film or a CMOS sensor *Schick CDR* (640 × 900 pixels, pixel size 38 μm) connected to a PC using the *CDR DICOM 5* software was used. In the latter case, the images were saved in RAW format for further analysis. Examples of static X-ray images of mechanical watches registered on the film and using the CMOS sensor are shown in Fig. 3. One can see that better spatial image resolution is achieved on the X-ray film. However, the sensitivity of the X-ray film was significantly lower than the sensitivity of the CMOS sensor, i.e., several tens of the generator shots were required to obtain a reliable image. Therefore, in dynamic experiments with exploding wires, only the CMOS sensor was used.

In the main part of the dynamic experiments, the objects studied were placed at the distance of 195 mm with respect to the anode, and the CMOS sensor was placed at the distance of 90 mm with respect to the object. This geometry defined the magnification of the system as 1.46. Also, because of the limited intensity of the X-ray flux, the typical level of the sensor's signal (pixel value) does not exceed 20% of its full dynamic range.

The spatial resolution was determined using an X-ray image of a target (see Fig. 4) consisting of 4 vertical and 4 horizontal tungsten wires of diameters 50, 100, 200, and 300 μm. In this experiment, the distance from the X-ray source to the phantom and from the target to the sensor was 135 mm and 45 mm, respectively. The X-ray effective focal

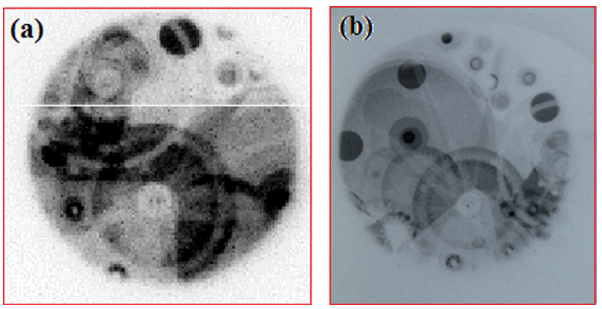

FIG. 3. Static x-ray images of mechanical watch obtained by (a) CMOS sensor and (b) X-ray film *Carestream E*.

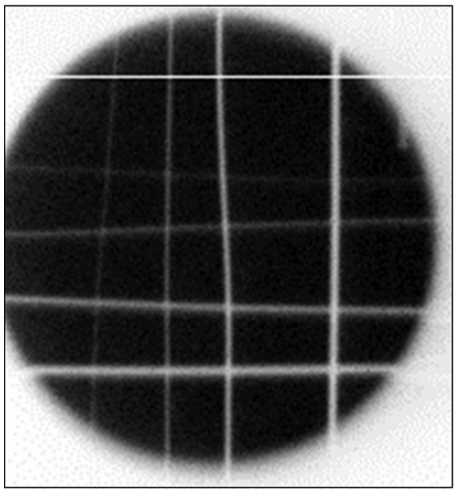

FIG. 4. X-ray images of tungsten wires of various diameters (left to right and top to bottom): 50, 100, 200, and 300 μm.

spot size can be estimated using the X-ray image of the wire and the known magnification of the setup. In Fig. 4, one can see that the vertical wire with 50 μm diameter is resolved. The width of the wire X-ray image at FWHM of its intensity was estimated as 170 ± 40 μm (4.5 ± 1 pixels). Considering the setup magnification, one obtains an effective X-ray horizontal spot size of ~0.3 mm. The X-ray image of the horizontal 50 μm diameter wire is noticeably weaker. The latter is related to significantly larger effective vertical size of the X-ray spot. Hence, in the present experiments, the value of 50 μm was considered as the minimal fully resolved distance in the horizontal direction.

The X-ray effective focal spot size was also determined following the European standard EN 12543–5.[33] An X-ray image of a copper plate (thickness of 0.1 mm) with a cross-like hole was obtained [see Fig. 5(a)], and the image intensity distributions in horizontal and vertical directions were analyzed. For each of distributions, the intensity level inside the hole was taken as 100%, and outside the hole (i.e., behind the copper plate), the level of the intensity was considered as 0%. Two pairs of markers were set at 16% and 50% of the maximal intensity [see Figs. 5(b) and 5(c)]. The sum of the intervals (in pixels) between these markers multiplied by the factor 1.4 and by the pixel size[33] can be used to determine the X-ray focal spot size in the vertical and horizontal directions as 1.35 ± 0.2 mm and 0.45 ± 0.2 mm, respectively. These values agree satisfactorily with the anode X-ray image, obtained using a 0.3-mm pinhole camera and an X-ray film [see Fig. 5(d)].

The sensitivity of the CMOS sensor to measure an areal density (g/cm^2) of the object was determined using a step wedge consisting of 6 layers of copper foils each of 60 μm thickness. The step wedge was placed in front of the CMOS sensor measurements. The level of darkness of the image was compared with the darkness level of the step wedge. These measurements showed that Cu foils with thickness in the range of 60–300 μm can be identified.

The complete experimental setup is shown in Fig. 6. The setup consists of an X-ray source, a μs-timescale compact high-current generator, and a stainless-steel chamber

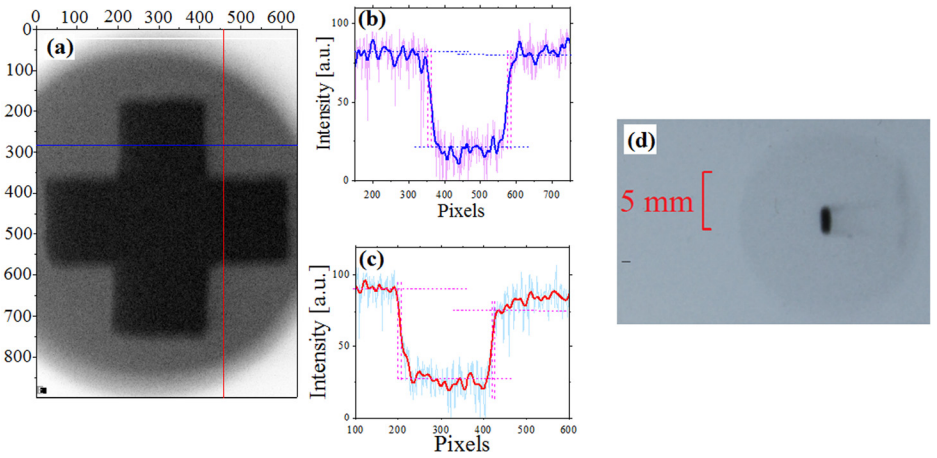

FIG. 5. (a) x-ray image of a copper plate with a cross-like hole; (b) vertical and (c) horizontal density profiles of the image edges; (d) x-ray image of the anode obtained on an x-ray film after 100 shots of the generator.

with two Perspex windows. A thin Perspex tube (inner and outer diameters of 7.4 and 9.8 mm, respectively), filled with de-ionized water, was placed coaxially inside the chamber and [Fig. 6(b)] a 60 mm long copper wire of 0.25 mm diameter was inserted along the axis of this dielectric tube and stretched between the HV and grounded electrodes.

The high-current generator consists of two capacitors, each of 0.51 μF, connected in parallel and charged up to 27 kV (stored energy 370 J). To discharge these capacitors, a triggered spark gap gas switch was used. The discharge current and the voltage at the load were measured by a Pierson current transformer and a Tektronix P6015A voltage divider, respectively. The waveforms of the current and voltage and PMT were registered and saved by a Tektronix TDS 784D digital oscilloscope (1 GHz, 4 Gs/s). To synchronize the operation of the magnetic system, the X-ray source, and the high-current generator, a Berkeley Nucleonics Corporation BNC 575 unit was used.

III. EXPERIMENTAL RESULTS

For a short-circuit load, the amplitude of the discharge current reaches ~27 kA with a rise time of 1.3 μs. In order to obtain a critically damped discharge where most of the stored energy is delivered to the wire within a time shorter than a quarter of a half period, several UEWEs were tested with different wire diameters and lengths. It was found that a 60 mm long Cu wire of 0.25 mm diameter satisfies the requirements of a critically damped discharge. Typical waveforms of the discharge current, voltage, and PMT signal, measured in the experiment, are shown in Fig. 7. One can see that the maximal current density reaches ~45 MA/cm^2. The total energy deposited into the exploding wire was ~300 J, which corresponds to a deposited energy density of ~12 kJ/g.

In Fig. 8, one can see a typical static, i.e., prior to the high-current generator shot, and dynamic X-ray images of the Cu wire and images of the step wedge obtained during the expansion phase of the exploding wire at different times relative to the beginning of the discharge current.

First, one can see that within a space resolution of 50 μm, there is no MHD and thermal instabilities like distortion of the axial symmetry and the formation of striations,[16] which are typical for wire explosions in vacuum or in gas. This agrees qualitatively with the data obtained in earlier research[27] and can be explained by smaller increments of these instabilities as compared with the case of the wire explosion in gas or vacuum. The latter is related to a significantly smaller radial expansion velocity of the exploding wire (~10^5 cm/s in water compared to ~10^7 cm/s in gas or vacuum), and consequently to larger density of the wire which determines increments in MHD ($m=0$) and thermal instabilities as $\propto \rho^{-0.5}$ and $\propto \rho^{-1}$, respectively.[15,19]

In comparison to laser shadow backlighting or the measurement of the wire's self-emission, X-ray imaging allows one to determine the radius of the wire at different times during the wire explosion without the error introduced by the shock wave formation. The measured time evolution of the wire diameter d is shown in Fig. 9 together with the results of one-dimension (1D) MHD simulation[34] coupled with EOS[7] for copper and water and a conductivity model.[9] One

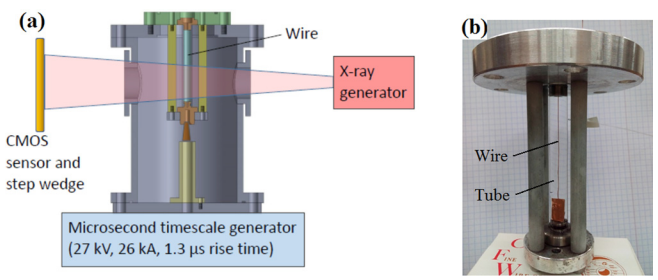

FIG. 6. (a) Experimental setup for microsecond timescale UEWE; (b) external view of the dielectric tube filled by de-ionized water with the Cu wire and holding electrodes.

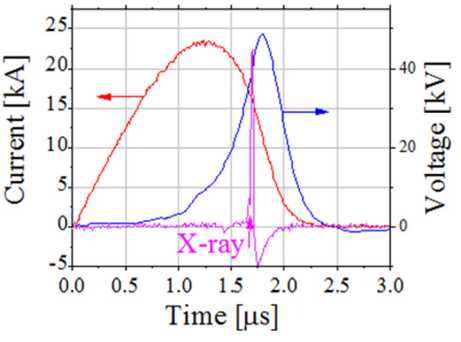

FIG. 7. Typical waveforms of current, voltage, and PMT signal.

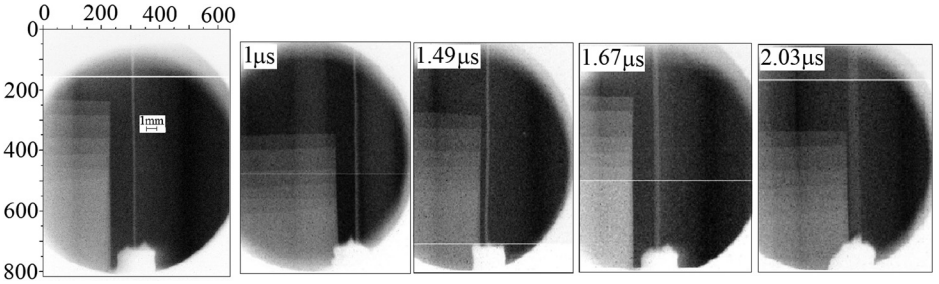

FIG. 8. Static (left) and dynamic x-ray images of Cu wires obtained at different time delays relative to the beginning of the discharge current.

can see a satisfactory agreement between the measured and simulated time evolution of the wire's radial expansion. A slightly smaller experimentally measured diameter than the simulation results can be explained by the mass density resolution of the X-ray imaging realized in the present experiments.

Next, the areal density, ρ_a, was determined using the grayscale contrast method, i.e., the radial distribution of grayscale level of the wire X-ray image was compared with the X-ray image of the step wedge blackness obtained at the same shot of the generator. The average density of the exploding wire ρ_{mean} can now be found using the known aerial density ρ_a which is measured near the wire's axis as $\rho_{mean} = \rho_a/d$. The average density of the wire can also be calculated using the measured diameter d of the wire at different times of the wire's explosion, $\rho_{calc} = \rho_0(d_0/d)^2$, where $\rho_0 = 8.96$ g/cm^3 and $d_0 = 0.25$ mm are the copper density at normal conditions and the initial diameter, respectively.

Time evolutions of ρ_{mean}, ρ_{calc}, and ρ_{MHD} are shown in Fig. 10. One can see that the values of the density calculated by these three methods agree satisfactorily well. At $d < 0.3$ mm, the grayscale contrast method leads to a smaller value of density than the calculated average density and its MHD simulation value because of the finite size of the X-ray hot spot [see Figs. 5(b) and 5(c)]. Thus, the grayscale contrast method can be used for reliable determination of the density distribution of the Cu wire with $d > 0.35$ mm for the given configuration.

The radial density distribution can also be obtained by an inverse Abel transform of the X-ray images. Indeed, the 1D projected intensity from a circularly symmetric emitter can be calculated using the Abel transform of the emission coefficient.[35] Therefore, the reconstruction of the circularly symmetric two-dimensional emission coefficient from its projection onto an axis can be achieved using the inverse Abel transformation of the projection. In our case, we wanted to reconstruct the density of the wire; therefore, we calculated the inverse Abel transformation of the function $F(y) = (1/\bar{\mu})ln[I_0/I(y)]$, where $\bar{\mu}$ is the average across the wavelength mass absorption coefficient, I_0 is the projected intensity outside the radius of the wire, and $I(y)$ is the projected intensity through the wire onto the y axis. This calculation was performed numerically using the algorithm described in Ref. 36. The experimental data were fitted with a 4th degree polynomial function and this function was used for the reconstruction of the density. This fitting was applied because of the finite space resolution and X-ray source size, which prevented the use of the raw data for the inverse Abel transform. Therefore, the obtained radial distribution of the density cannot be considered reliable above a certain radius of the wire for each moment of the explosion. An example of this analysis, i.e., the radial density distribution at $t = 1.45$ μs together with the results of 1D MHD simulations, is shown in Fig. 11, where the red dots represent the range of the calculation where the results are not reliable. One can see that the results of the inverse Abel transform and 1D MHD modeling (in the reliable range) are in a satisfactory agreement and show almost uniform radial density distribution. The latter allows the application of the simple grayscale contrast method for the radial density distribution for this case of the Cu wire explosion.

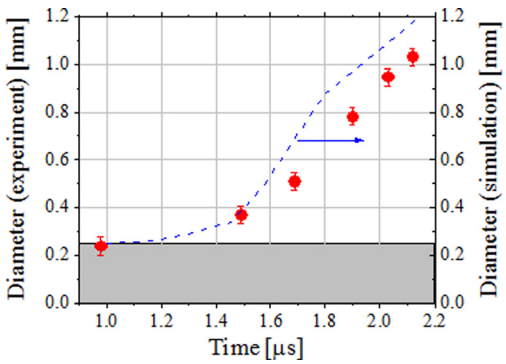

FIG. 9. The Cu wire diameter at different times of the wire explosion. Circles – measured diameter of the wire d; dashed line – the wire diameter obtained by the 1D MHD simulation. The upper border of the gray area corresponds to the initial wire diameter.

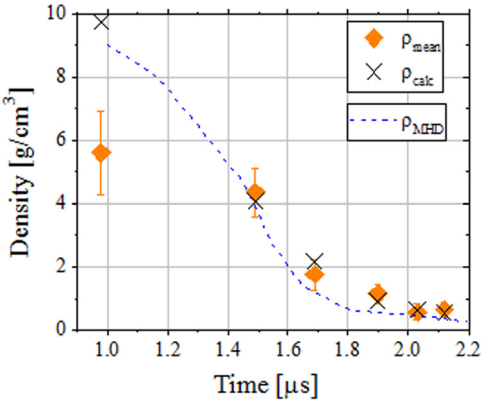

FIG. 10. Time dependence of the density of the exploding wire: ρ_{mean} is the average density measured by the grayscale contrast method; ρ_{calc} is the density calculated from the measured diameter; ρ_{MHD} is the density at radius 0.1 mm, obtained by the 1D MHD simulation.

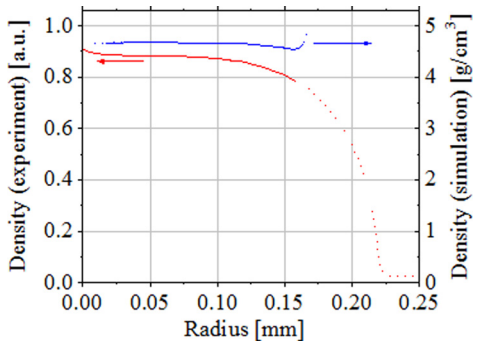

FIG. 11. Radial distribution of the density of an exploding wire at $t = 1.45$ μs. Red line: results based on inverse Abel transform. Blue line: results of MHD simulation. Dots represent the unreliable range of the calculation.

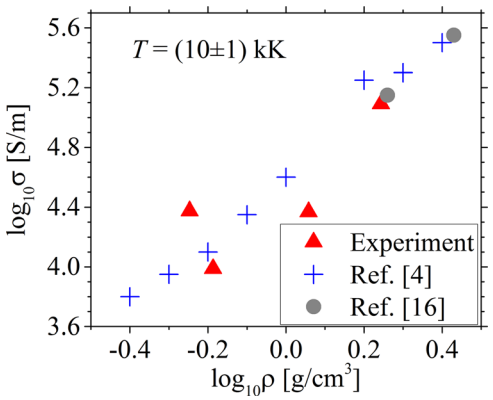

FIG. 12. Experimentally measured conductivity of copper plasma for $T = 10$ kK. Triangles—present research; crosses—Ref. 4; circles—Ref. 16.

IV. DISCUSSION

Using 1D MHD simulation[34] coupled with SESAME[7] EOS for copper, Bakulin-Kuropatenko-Luchinskii (BKL) conductivity model,[9] Ohm's law, thermal diffusion equation where values of heat transfer coefficients are found from the Wiedemann-Franz law and electrical circuit equation, and a satisfactory good fitting between the simulated and experimental waveforms of the current and voltage were obtained with only small variations of conductivity data. A good agreement between the simulated and measured radial expansion of the exploding wire was obtained as well. In addition, a uniform radial density distribution obtained by the inverse Abel transform agrees with the results of the MHD simulation. Thus, one can conclude that the SESAME EOS for copper and the BKL conductivity model in this range of input rate of the energy density $d\varepsilon/dt \leq 0.04\,\mathrm{eV/(atom\,ns)}$ are valid.

The 1D MHD simulation of a Cu wire electrical explosion showed that the radial temperature distribution is almost uniform (except for a $\sim$20 μm thick layer adjacent to the water where the temperature decreases by $\sim$30%). The absolute value of the temperature increases up to 9 kK at 1.6 μs, and for the next 0.8 μs, it remains in the range (10 ± 1) kK. This value of temperature together with the measured density corresponds to the plasma with a coupling parameter $\Gamma = (Ze)^2/[4\pi\varepsilon_0 3^{1/3}(4\pi n_i)^{-1/3}k_BT] \approx 0.4$, where Z is the ionization state of the ion ($\sim$1 for the temperature range considered), k_B is the Boltzmann coefficient, ε_0 is the absolute dielectric constant, and n_i is the ion density which can be determined using the Saha formula for the low-ionized plasma, $n_1 = n_e \approx \sqrt{2}n_a^{1/2}(g_1/g_0)^{1/2}\lambda^{-3/2}\exp(E_{ion}/k_BT)$. Here, g_0 and g_1 are the degeneracy of the ground states of the Cu I atom and Cu II ion, respectively, $E_{ion} = 7.726$ eV is the ionization energy of the Cu atom and $\lambda^2 = [h^2/(2\pi m_e k_B T)]$ is the thermal de Broglie wavelength of an electron, h is Planck's constant, and m_e is the electron mass.

Finally, data regarding the electrical conductivity as a function of the copper density for the evaluated temperature, $T = 10$ kK, were obtained using the measured resistance and diameter of the exploding wire. These data together with the data calculated in earlier studies[4,16] at $T = 10$ kK are shown in Fig. 12. One can see that the conductivity values, calculated in the present research, agree satisfactorily with the numerical data obtained in the earlier research where only optical and electrical diagnostics were used. This is expected because of the good fit between the experimental and numerical simulation results.

V. SUMMARY

In this paper, we presented the results of the first space- and time-resolved density distribution of the copper wire during its microsecond timescale underwater electrical explosion, observed using X-ray backlight imaging. A flash X-ray source generates a 20-ns pulse of X-ray flux with a significant part of the X-rays having energies >60 keV. Using a conventional CMOS sensor, the X-ray image of 50-μm tungsten wire was resolved.

The obtained X-ray images of the exploding Cu wire showed the absence of MHD and thermal instabilities on a scale $\geq$50 μm, as well as the absence of detectable density gradients. The density measurements by the grayscale-contrast method give a reasonable agreement with the results of a 1D MHD simulation. The latter showed that the exploding wire reaches a temperature of $T = 10$ kK at $t = (1.6$–$2.4)$ μs. For this temperature, the conductivity of warm dense copper plasma was evaluated and found in a good agreement with earlier obtained data from experiments where only electrical and optical diagnostics were applied to obtain the exploding wire parameters.

In addition, the 1D MHD simulations show a satisfactory agreement between the simulated and experimental waveforms of the current and the voltage and the measured radial expansion of the exploding wire. Also, the radial density distribution obtained by the inverse Abel transform agrees with the results of MHD simulations. These results confirm the validity of the SESAME EOS for copper and the BKL conductivity model used in the MHD simulations for the parameters of the exploding wire realized in the present research.

In the near future, we plan to conduct experiments with increased brightness, smaller X-ray source size, and decreased distance between the sensor and the exploding wire. These experiments will be carried out using ns-timescale UEWE and will allow us to obtain time- and space-resolved radial distributions of density. The latter will allow us to study possible non-uniformities of the exploding wire in the ns-time scale.

ACKNOWLEDGMENTS

We thank Dr. S. Bland and Dr. J. Leopold for critical reading and helpful comments. This research was supported by the Center for Absorption in Science, Ministry of Immigrant Absorption, State of Israel.

[1]V. Luchinskii, *Electrical Explosion of Wires* (Nauka, Moscow, Russia, 1989).
[2]V. E. Fortov and I. T. Iakubov, *The Physics of Non-Ideal Plasma* (World Scientific, Singapore, 2000).
[3]A. W. DeSilva and H.-J. Kunze, Phys. Rev. E **49**, 4448 (1994).
[4]A. W. DeSilva and J. D. Katsouros, Phys. Rev. E **57**, 5945 (1998).
[5]Y. E. Krasik, S. Efimov, D. Sheftman, A. Fedotov-Gefen, O. Antonov, D. Shafer, D. Yanuka, M. Nitishinskiy, M. Kozlov, L. Gilburd, G. Toker, S. Gleizer, E. Zvulun, V. T. Gurovich, D. Varentsov, and M. Rodionova, IEEE Trans. Plasma Sci. **44**, 412 (2016).
[6]V. Oreshkin, R. B. Baksht, A. Y. Labezkii, A. G. Rousskikh, A. V. Shishlov, P. R. Levashov, K. V. Khishchenko, and I. V. Glazyrin, Tech. Phys. **49**, 843 (2004).
[7]*SESAME: The Los Alamos National Laboratory Equation of State Database*, edited by S. P. Lyon and J. D. Johnson, Report No. LA-UR-92-3407, Group T-1.
[8]R. M. More, K. H. Warren, D. A. Young, and G. B. Zimmerman, Phys. Fluids **31**, 3059 (1988).
[9]Y. D. Bakulin, V. F. Kuropatenko, and A. V. Luchinskii, Sov. Phys. Tech. Phys. **21**, 1144 (1976).
[10]Y. T. Lee and R. M. More, Phys. Fluids **27**, 1273 (1984).
[11]S. Ichimaru and S. Tanaka, Phys. Rev. A **32**, 1790 (1985).
[12]R. Redmer, Phys. Rev. E **59**, 1073 (1999).
[13]M. P. Desjarlais, Contrib. Plasma Phys. **41**, 267 (2001).
[14]M. P. Desjarlais, J. D. Kress, and L. A. Collins, Phys. Rev. E **66**, 025401 (2002).
[15]D. Sheftman and Y. E. Krasik, Phys. Plasmas **17**, 112702 (2010).
[16]D. Sheftman and Y. E. Krasik, Phys. Plasmas **18**, 092704 (2011).
[17]D. Sheftman, D. Shafer, S. Efimov, and Y. E. Krasik, Phys. Plasmas **19**, 034501 (2012).
[18]H. Bluhm, *Pulsed Power Systems: Principles and Applications* (Springer-Verlag, Berlin, Heidelberg, 2006).
[19]V. I. Oreshkin, Phys. Plasmas **15**, 092103 (2008).
[20]A. W. DeSilva and G. B. Vunni, Phys. Rev. E **83**, 037402 (2011).
[21]T. Sasaki, M. Nakajima, T. Kawamura, and K. Horioka, Phys. Plasmas **17**, 084501 (2010).
[22]J. Clérouin, P. Noiret, P. Blottiau, V. Recoules, B. Siberchicot, P. Renaudin, C. Blancard, G. Faussurier, B. Holst, and C. E. Starrett, Phys. Plasmas **19**, 082702 (2012).
[23]J. Stephens and A. Neuber, Phys. Rev. E **86**, 066409 (2012).
[24]S. A. Pikuz, T. A. Shelkovenko, A. R. Mingaleev, D. A. Hammer, and H. P. Neves, Phys. Plasmas **6**, 4272 (1999).
[25]T. A. Shelkovenko, S. A. Pikuz, and D. A. Hammer, Plasma Phys. Rep. **42**, 226 (2016).
[26]X. Zhu, X. Zou, S. Zhao, H. Shi, R. Zhang, H. Luo, and X. Wang, IEEE Trans. Plasma Sci. **42**, 2522 (2014).
[27]D. Sheftman, D. Shafer, S. Efimov, K. Gruzinsky, S. Gleizer, and Y. E. Krasik, Rev. Sci. Instrum. **83**, 103505 (2012).
[28]D. Varentsov, O. Antonov, A. Bakhmutova, C. W. Barnes, A. Bogdanov, C. R. Danly, S. Efimov, M. Endres, A. Fertman, A. A. Golubev, D. H. H. Hoffmann, B. Ionita, A. Kantsyrev, Y. E. Krasik, P. M. Lang, I. Lomonosov, F. G. Mariam, N. Markov, F. E. Merrill, V. B. Mintsev, D. Nikolaev, V. Panyushkin, M. Rodionova, M. Schanz, K. Schoenberg, A. Semennikov, L. Shestov, V. S. Skachkov, V. Turtikov, S. Udrea, O. Vasylyev, K. Weyrich, C. Wilde, and A. Zubareva, Rev. Sci. Instrum. **87**, 023303 (2016).
[29]S. N. Rukin, Instrum. Exp. Tech. **4**, 439 (1999).
[30]G. A. Mesyats, *Explosive Electron Emission* (URO, Ekaterinburg, 1998).
[31]Y. Hadas, A. Sayapin, Y. E. Krasik, V. Bernshtam, and I. Schnitzer, J. Appl. Phys. **104**, 064125 (2008).
[32]See https://www.nist.gov/pml/X-ray-mass-attenuation-coefficients for NIST database.
[33]European Committee for Standardization, EN 12543–5, E. Brussels, 1999.
[34]A. Grinenko, Y. E. Krasik, S. Efimov, A. Fedotov, V. T. Gurovich, and V. I. Oreshkin, Phys. Plasmas **13**, 042701 (2006).
[35]H. R. Griem, *Principles of Plasma Spectroscopy* (Cambridge University Press, 1997).
[36]L. M. Smith, D. R. Keefer, and S. I. Sudharsanan, J. Quant. Spectrosc. Radiat. Transfer **39**, 367 (1988).